



Analysis of a New Rocket-Based Combined-Cycle Engine Concept at Low Speed

S. Yungster
Institute for Computational Mechanics in Propulsion, Cleveland, Ohio

C.J. Trefny
Glenn Research Center, Cleveland, Ohio

Prepared for the
35th Joint Propulsion Conference and Exhibit
cosponsored by AIAA, ASME, SAE, and ASEE
Los Angeles, California, June 20-24, 1999

Prepared under Cooperative Agreement NCC3-542

National Aeronautics and
Space Administration

Glenn Research Center

Acknowledgments

The authors would like to acknowledge K. Radhakrishnan, of the Institute for Computational Mechanics in Propulsion (ICOMP), for providing us with the chemical equilibrium subroutines and for his help during their implementation into the present code; and C.A. Snyder of NASA Glenn Research Center, for providing us with the performance data for the SMC cycle.

Available from

NASA Center for Aerospace Information
7121 Standard Drive
Hanover, MD 21076
Price Code: A03

National Technical Information Service
5285 Port Royal Road
Springfield, VA 22100
Price Code: A03

ANALYSIS OF A NEW ROCKET-BASED COMBINED-CYCLE ENGINE CONCEPT AT LOW SPEED

S. Yungster

Institute for Computational Mechanics in Propulsion
Cleveland, Ohio 44135

C.J. Trefny

National Aeronautics and Space Administration
Glenn Research Center
Cleveland, Ohio 44135

Abstract

An analysis of the Independent Ramjet Stream (IRS) cycle is presented. The IRS cycle is a variation of the conventional ejector-ramjet, and is used at low speed in a rocket-based combined-cycle (RBCC) propulsion system. In this new cycle, complete mixing between the rocket and ramjet streams is not required, and a single rocket chamber can be used without a long mixing duct. Furthermore, this concept allows flexibility in controlling the thermal choke process. The resulting propulsion system is intended to be simpler, more robust, and lighter than an ejector-ramjet. The performance characteristics of the IRS cycle are analyzed for a new single-stage-to-orbit (SSTO) launch vehicle concept, known as "Trailblazer." The study is based on a quasi-one-dimensional model of the rocket and air streams at speeds ranging from lift-off to Mach 3. The numerical formulation is described in detail. A performance comparison between the IRS and ejector-ramjet cycles is also presented.

Introduction

The NASA Glenn Research Center is currently developing a reusable, single-stage-to-orbit (SSTO) launch vehicle known as "Trailblazer" that utilizes a rocket-based combined-cycle (RBCC) propulsion system. This vehicle, shown in Fig. 1, will operate in four modes from lift-off to orbit: 1) air-augmented rocket, 2) ramjet, 3) supersonic combustion ramjet (scramjet), and 4) all-rocket. The Trailblazer is an axisymmetric vehicle having three RBCC propulsion pods equally-spaced at 120° intervals. This configuration insures that the total thrust vector is always aligned with the vehicle's axis, and allows the forebody boundary layer to be diverted between the pods. An axisymmetric vehicle was chosen in part, for its high structural and volumetric efficiency, and for its low drag, at the cost of lower inlet pre-compression. The entire cross-sectional area of the vehicle is available for nozzle expansion. A detailed description of the Trailblazer vehicle is given in Ref. 1.

A propulsion system using the ramjet and scramjet cycles must have another means of acceleration from static conditions to low supersonic speeds, at which point the ramjet cycle can generate sufficient thrust for further acceleration. RBCC systems use rocket motors to accomplish this, and are characterized by a high degree of integration between the rocket and ramjet cycles. This integration can provide both thermodynamic and structural advantages over a system in which the rocket and ramjet engines are separate. Some form of RBCC propulsion is generally considered to be an appropriate choice for air-breathing, reusable, SSTO launch vehicles².

In this study, we focus on the low speed mode which typically covers the speed range from lift-off to a maximum around Mach 3. Two general classes of RBCC engines appear in the literature, diffusion and afterburning (DAB), and simultaneous mixing and combustion (SMC). They are distinguished by their thermodynamic cycle. In the DAB cycle, an inert rocket exhaust is used as the primary flow in an ejector process. Following ejector pumping, the mixed flow is diffused, fueled and burned subsonically in an afterburner. Subsequently, the gases are expanded through a convergent-divergent nozzle. This scheme results in high thermodynamic performance, but due to the serial nature of the processes, requires a long duct and suffers from low thrust-to-weight ratio. Any combustion during the mixing process reduces performance, so a stoichiometric or oxygen-rich rocket exhaust is generally assumed. The use of a number of small primary nozzles can shorten the required mixing duct length, but the design of small, stoichiometric rocket nozzles raises numerous issues related to structural and thermal design and reliability.

Some of the negative aspects of the DAB cycle are eliminated at the expense of some thermodynamic performance with the SMC cycle. In the SMC cycle, the rocket exhaust is fuel-rich and provides some fraction of the fuel required for combustion with the entrained airflow. The rocket and air streams mix and burn simultaneously, eliminating the need for a diffuser and afterburner duct. This process generally results in thermal choking where mixing is complete, fol-

lowed by expansion through the remaining area ratio. A convergent-divergent nozzle is not required, making this cycle more practical for RBCC engines designed to operate also in scramjet mode. However, the requirement for complete mixing of the rocket and air streams still results in very long mixing/combustor ducts. For example, the studies of Dimotakis³ indicate that, for typical conditions in an RBCC engine at $M_0 = 1$, complete mixing may be reached within an axial distance of between 7 and 13 duct heights (for a rectangular configuration).

This paper presents an RBCC engine concept that is directed even further toward the potential for high structural efficiency and minimum complexity by employing a low speed cycle in which the rocket and ramjet streams do not mix. Removing the requirement for mixing can shorten the flowpath considerably, with a corresponding reduction in structural weight and wetted area. Another benefit is a reduction in risk and complexity since a single rocket element can now be used without regard for mixing length. Also, higher thermodynamic performance is possible in other modes where a shorter mixing duct would reduce expansion process losses.

In this new "Independent Ramjet Stream" (IRS) cycle, the airstream is fueled independently using the ramjet and scramjet mode fuel injectors located in the inlet diffuser, as shown in Fig. 2a. This can be accomplished upstream, since the air stagnation temperatures during this mode are not high enough to cause autoignition. The rocket will serve as a pilot for the fueled airstream. At the point of ignition, a flame propagates across the ramjet duct forming a thermal throat. The length of the flowpath is now determined by the flame propagation speed. Since the rocket is not the fuel source for the airstream, the rocket oxidizer-to-fuel ratio (O/F) can be fixed at an optimum value for best system performance. An additional advantage of the IRS cycle is that the fuel injectors provide the means to control the location of the thermal throat by adjusting the amount and radial distribution of the fuel injected into the airstream.

The objective of this work is to describe a computational analysis tool developed for the IRS cycle, and investigate the performance of this propulsion mode over its operating flight range ($0 \leq M_0 \leq 3$). An additional objective is to generate performance maps for trajectory optimization.

Numerical Formulation

The ramjet and rocket streams are solved simultaneously using a total variation diminishing (TVD) MacCormack time-marching scheme⁴. It is assumed that the primary (rocket) and secondary streams do not mix, and therefore, each stream can be computed independently. The only interaction between the primary and secondary streams occurs through a matched-pressure interface.

A quasi-one dimensional approximation is used to model both streams. Combustion in the ramjet stream is modeled by a prescribed distribution of hydrogen fuel along the combustor duct as described later. Equilibrium chemistry is used to model the combustion process utilizing the LSENS kinetics code of Radhakrishnan⁵. The pressure matching is accomplished in the present work, by adding an auxiliary equation for the area of the primary stream, A_p .

The quasi one-dimensional Euler equations in conservation law form for the two streams, and the auxiliary equation can be expressed as

$$\frac{\partial \mathbf{Q}}{\partial t} + \frac{\partial \mathbf{F}}{\partial x} = \mathbf{S} \quad (1)$$

where the vectors \mathbf{Q} , \mathbf{F} and \mathbf{S} are

$$\mathbf{Q} = \begin{bmatrix} \rho_p \\ m_p \\ e_p \\ \rho_s \\ m_s \\ e_s \\ A_p \end{bmatrix}; \quad \mathbf{F} = \begin{bmatrix} m_p \\ m_p^2/\rho_p + p_p \\ (e_p + p_p)m_p/\rho_p \\ m_s \\ m_s^2/\rho_s + p_s \\ (e_s + p_s)m_s/\rho_s \\ 0 \end{bmatrix}; \quad \mathbf{S} = \begin{bmatrix} 0 \\ \rho_p \frac{dA_p}{dx} \\ 0 \\ 0 \\ \rho_s \frac{dA_s}{dx} \\ \rho_s \dot{q} A_s \\ K\delta(p_p - p_s) \end{bmatrix} \quad (2)$$

The dependent variables are the mass density ρ , the momentum m (equal to ρu , where u is the velocity), and the total energy per unit volume e . The subscripts 'p' and 's' denote the primary (rocket) and secondary streams respectively. The last dependent variable is the primary stream area A_p . The sum of the primary and secondary areas must equal the prescribed total engine area, A_{tot} , at every point. That is

$$A_p(x) + A_s(x) = A_{tot}(x) \quad (3)$$

The term \dot{q} denotes the external rate of heat addition per unit mass. This term includes only the heat that is added externally and does not include heat released by chemical reactions. The variable K is a constant that controls the rate of change of the primary area ($0 < K < 0.5$ in this study), and δ is a function of the primary Mach number, M_p , given by

$$\delta = \begin{cases} 1 & \text{if } M_p > 1 \\ -1 & \text{if } M_p < 1 \end{cases} \quad (4)$$

An additional equation is needed to relate the pressure to the flow variables ρ , m , and e . From the definition of static enthalpy per unit mass, h , we have the following relation

$$h = \varepsilon + p/\rho \quad (5)$$

where ε is the internal energy per unit mass. The parameter $\tilde{\beta}$ is introduced and defined as the ratio of static enthalpy to internal energy

$$\tilde{\beta} = \frac{h}{\varepsilon} \quad (6)$$

The total energy can be written as the sum of the internal energy and kinetic energy

$$e/\rho = \varepsilon + \frac{1}{2}u^2 \quad (7)$$

Combining Eqs. (5)-(7) yields the desired relationship

$$p = (\tilde{\beta} - 1)(e - \frac{1}{2}\rho u^2) \quad (8)$$

Equation (8) is a general expression valid for any gas mixture. The parameter $\tilde{\beta}$ is a property of the gas and in general depends on its pressure, temperature and species composition. For an ideal gas, $\tilde{\beta}$ equals the ratio of specific heats, γ . For a gas that is in chemical equilibrium, the parameter $\tilde{\beta}$ is calculated, in this study, using the equilibrium composition method developed by Gordon and McBride⁶, and using the implementation of Radhakrishnan as given in the LSENS chemical kinetics code⁵. The chemical equilibrium state for a given initial mixture composition can be obtained when any two independent thermodynamic state variables are specified. In the present code, we compute the equilibrium composition based on two sets of variables: specific internal energy and specific volume density (UV), and temperature and pressure (TP). The chemical equilibrium state is computed for the TP problem by minimizing the Gibbs function, and for the UV problem by minimizing the Helmholtz function. A Detailed description of the equations and solution procedure used to compute the chemical equilibrium state is given by Radhakrishnan⁵.

Numerical Method

The numerical method selected for solving the quasi one-dimensional Euler equations is the explicit, second-order, Total Variation Diminishing (TVD) MacCormack scheme⁴. The auxiliary primary area equation is integrated using a simple Euler method. The TVD MacCormack scheme can be

written as follows:

$$\Delta Q_j^{(1)} = -\frac{\Delta t}{\Delta x}(F_j^n - F_{j-1}^n) + \Delta t S_j^n \quad (9)$$

$$Q_j^{(1)} = \Delta Q_j^{(1)} + Q_j^n \quad (10)$$

$$\Delta Q_j^{(2)} = \frac{1}{2} \left[-\Delta Q_j^{(1)} - \frac{\Delta t}{\Delta x}(F_{j+1}^{(1)} - F_j^{(1)}) + \Delta t S_j^{(1)} \right] \quad (11)$$

$$Q_j^{(2)} = \Delta Q_j^{(2)} + Q_j^{(1)} \quad (12)$$

$$Q_j^{n+1} = Q_j^{(2)} + (X_{j+1/2}^n \Phi_{j+1/2}^n - X_{j-1/2}^n \Phi_{j-1/2}^n) \quad (13)$$

The first two steps (Eqs. 9-12) represent the standard MacCormack scheme where the superscripts "(1)" and "(2)" designate values of the function evaluated at the intermediate solutions $Q^{(1)}$ (predictor step) and $Q^{(2)}$ (corrector step). The last step (Eq. 12) represents an additional conservative dissipation designed in such a way that the final scheme satisfies the TVD conditions (see Ref. 7). Let $A = (\partial F)/(\partial Q)$, then the vector $X_{j+1/2}^n$ in Eq. (13) denotes the matrix of eigenvectors of the flux Jacobian matrix A evaluated at some symmetric average of Q_j and Q_{j+1} denoted as $Q_{j+1/2}$. In the present work we use a symmetric TVD scheme for which the elements of the vector $\Phi_{j+1/2}^n$, denoted by $\phi_{j+1/2}^l$ are given by:

$$\phi_{j+1/2}^l = \frac{1}{2} [\Psi(v_{j+1/2}^l) - (v_{j+1/2}^l)^2] (\alpha_{j+1/2}^l - \Theta_{j+1/2}^l) \quad (14)$$

$$v_{j+1/2}^l = \frac{\Delta t}{\Delta x} a_{j+1/2}^l \quad (15)$$

Here $a_{j+1/2}^l$ denotes the eigenvalues of the Jacobian matrix A evaluated at $Q_{j+1/2}$, and $\alpha_{j+1/2}^l$ denotes the elements of the vector $\alpha_{j+1/2}$:

$$\alpha_{j+1/2} = X_{j+1/2}^{-1} (Q_{j+1} - Q_j) \quad (16)$$

The function Ψ is:

$$\Psi(z) = \begin{cases} |z| & |z| \geq \varepsilon \\ \frac{(z^2 + \varepsilon^2)}{2\varepsilon} & |z| < \varepsilon \end{cases} \quad (17)$$

The entropy correction parameter, ε , in Eq. (17) is taken to be a small positive number in the range $0.05 \leq \varepsilon \leq 0.25$. A value of $\varepsilon = 0.125$ was used in the present work. The limiter function $\Theta'_{j+1/2}$ used in this study is the following:

$$\Theta'_{j+1/2} = \text{minmod}(\alpha'_{j-1/2}, \alpha'_{j+1/2}, \alpha'_{j+3/2}) \quad (18)$$

The expressions for the eigenvalues and eigenvectors are given in the Appendix.

Heat Release Distribution

A brief description of the combustion process in the IRS cycle is needed in order to understand the heat release model adopted in this work. In the IRS cycle, fuel injectors located in the inlet diffuser are used to distribute fuel into the airstream. The premixed stream is then ignited by contact with the hot rocket plume, and a flame propagates across the secondary stream. The combustion is completed at some point before the end of the ramjet duct. If the fuel is distributed in such a way that it does not penetrate completely across the duct and instead a thin layer of noncombustible gas exists between the rocket plume and the fueled airstream, then some mixing and diffusion must take place for ignition to occur. This radial distribution of fuel can therefore be used to control the point of ignition, and therefore the thermal throat location.

In the present quasi-one dimensional analysis, we model the combustion process by specifying an ignition point, x_q^{st} , an end of heat release point, x_q^{en} , and a distribution function between them. For ideal gas calculations, the heat release distribution is specified by the source term $\dot{q}(x)$, where the total heat added per unit time is given by $\int \rho_s \dot{q} dV$. For equilibrium flow calculations, the heat release distribution is specified as follows. Consider a case where the fuel is hydrogen. Then, we define a new chemical species named "inert hydrogen" which has identical properties as "real" hydrogen with the exception that inert hydrogen does not participate in any chemical reactions. The total hydrogen concentration at any given point is then given by the sum of inert and real hydrogen. By prescribing the axial distribution of real hydrogen along the flow domain we can specify the heat release distribution, and at the same time introduce a combustion efficiency (by specifying a nonzero value for the inert hydrogen at the end of the combustion process). For the RBCC computations, the following cubic function was used to express the real hydrogen mole concentration

$$n_{H2} = \eta_c \phi \left[\left(3 - \frac{1}{\Delta x_q} \right) z^2 + \left(\frac{1}{\Delta x_q} - 2 \right) z^3 \right]; \quad 0 \leq z \leq 1 \quad (19)$$

where η_c is the combustion efficiency, ϕ is the equivalence ratio, $\Delta x_q = x_q^{en} - x_q^{st}$ is the length of the heat release zone, and z is the nondimensional distance, $z = (x - x_q^{st}) / (\Delta x_q)$.

Results

The accuracy of the method is first demonstrated by presenting computations for two benchmark cases, involving reacting and nonreacting flows. They are presented below.

Benchmark test cases

The first case considers the nonreacting flow of an ideal gas in a divergent nozzle. We use the unsteady quasi-one dimensional Euler equations to obtain the steady-state solution for an inflow Mach number $M_1 = 1.25$ and a back pressure $p_b = 1.87466 p_1$, where p_1 is the static pressure at the inflow plane. The area distribution $A(x)$ of the divergent nozzle considered is given in Fig. 3, which compares the CFD result with the exact analytical solution. For these flow conditions, a normal shock forms at the midpoint of the nozzle ($x = 0.5$). The CFD solution was computed on a 200 point grid and demonstrates the accuracy of the TVD scheme, which leads to sharp stationary shock transitions, over two grid points.

The second test case considers thermal choking in a classical Rayleigh flow, which consists of frictionless, one dimensional flow in a constant area duct with heat addition. Calculations were performed for an inflow gas mixture of hydrogen-air having a fuel-air ratio of $f/a = 0.00152$, and a sufficiently low exit pressure to cause thermal choking. If we assume that the hydrogen-air mixture behaves as an ideal gas, then an exact analytical solution exists for this problem (Ref. 9). The total temperature ratio T_{t2}/T_{t1} between the exit and entrance to the duct can then be easily computed to be $T_{t2}/T_{t1} = 1.4464$ for this fuel-air ratio. For a choked flow ($M_2 = 1.0$), the inflow Mach number, M_1 , is analytically computed to be $M_1 = 0.5$, and the corresponding total pressure loss is $p_{t2}/p_{t1} = 0.8976$.

Figure 4 shows the CFD results for the above conditions assuming an ideal gas. The external heat is added from stations $x = 0.25$ to $x = 0.75$. The computed inflow Mach number is $M_1 = 0.5004$, and the computed total temperature and total pressure ratios are $T_{t2}/T_{t1} = 1.4452$, and $p_{t2}/p_{t1} = 0.8978$ respectively, which are in excellent agreement with the analytical solution.

The calculation was repeated for the same fuel-air ratio but without the assumption of ideal gas, and considering instead a real gas in chemical equilibrium. The heat release zone considered was from $x_q^{st} = 0.25$ to $x_q^{en} = 0.75$, using a cubic function slightly different from the one given in Eq. 19, and different also from the distribution assumed in the ideal gas calculation. (We should point out that for this case, the inflow and outflow states are independent of the assumed heat release distribution.) The results are shown in Fig. 5, which compares the pressure, temperature and Mach number distribution for equilibrium and ideal gas flows. The computed inflow Mach number for the equilibrium calculation is slightly higher than the theoretical value of $M_1 = 0.5$, probably due to a small amount of dissociation at the exit plane which results in a slightly lower amount of effective heat release. The assumption of a constant specific heat in the ideal gas calculation may contribute also to the small differences observed between the ideal gas and equilibrium flow calculations.

Analysis of a Trailblazer RBCC engine at low speed

We investigated the performance characteristics of the IRS cycle for a specific Trailblazer configuration over the flight Mach number range of $0 \leq M_0 \leq 3$. All computations were carried out with equilibrium chemistry.

Referring to the control volume shown in Fig. 2b, the net thrust is calculated by

$$F_{net} = F_{gross} - F_{ram} - F_{inlet} \quad (20)$$

The first term on the right hand side of Eq. (20) is the gross thrust, and is computed as follows

$$F_{ideal} = \rho_9 u_9^2 A_9 \quad (21)$$

$$F_{gross} = C_{fg} F_{ideal} \quad (22)$$

where C_{fg} is the nozzle gross thrust coefficient. The second term on the right hand side of Eq. (20) is the ram drag, and can be written as

$$F_{ram} = \rho_1 u_1^2 A_1 \quad (23)$$

The final term in Eq. (20) represents the inlet drag which includes the contributions from spillage, cowl lip and diverter drag, and is obtained from the two-dimensional CFD calculations of the inlet reported by DeBonis *et al*⁸.

The net specific impulse, I_{sp} , is then calculated by

$$I_{sp} = \frac{F_{net}}{\dot{w}_p + (\dot{w}_{fuel})_s} \quad (24)$$

Here, \dot{w}_p is the propellant weight flow rate for the primary stream, and $(\dot{w}_{fuel})_s$ is the fuel weight flow rate for the secondary stream.

The rocket element is designed to operate at a constant O/F ratio but at variable chamber pressure. Therefore, we investigated the performance of the IRS cycle at different chamber pressures, p_c , in the range $100 \leq p_c/p_0 \leq 350$, where p_0 is the free-stream pressure. The design parameters for the configuration studied are given below:

$$\text{Capture area (per pod)} A_c = 18094.7 \text{ in}^2$$

$$\text{Ramjet duct inlet total area ratio } A_3/A_c = 0.4$$

$$\text{Ramjet duct exit area ratio } A_6/A_c = 1.25$$

$$\text{Ramjet duct nondimensional length } L/A_c^{1/2} = 2.1452$$

$$\text{Ramjet duct inlet secondary area ratio } A_{3s}/A_c = 0.3318$$

$$\text{Rocket O/F ratio} = 6.0$$

$$\text{Rocket throat area ratio } A^*/A_c = 0.0068$$

$$\text{Rocket exit area ratio } A_{3p}/A^* = 10.0$$

$$\text{Maximum combustion efficiency } \eta_c = 0.95$$

The calculations assumed that the rocket (primary) flow was frozen from the throat downstream, and that the secondary flow is in chemical equilibrium. The heat release distribution was based on the cubic function given in Eq. (19). The CFD computations were carried out from station 3 to station 6 (see Fig. 2b). An isentropic expansion to free-stream conditions was assumed from station 6 to station 9. Expansion losses were included in the nozzle gross thrust coefficient C_{fg} . The values assumed for C_{fg} are given in Table 1.

The boundary conditions were specified as follows. At the inflow plane (station 3 in Fig. 2b), the primary stream pressure, temperature, Mach number and gas properties were specified. For the secondary stream, the total pressure, total temperature and fuel-air ratio was specified. Total pressure values were based on the inlet recovery of Ref. 8. At the outflow boundary (station 6), the outflow pressure was imposed if the flow was subsonic, and all the variables were extrapolated if the flow was supersonic.

Since the maximum amount of air flowing into the engine is known at every Mach number from the CFD inlet

calculations⁸, the fuel-air ratio in the secondary stream, and/or the heat release distribution were adjusted to match this given airflow.

Figures 6 and 7 show typical flow properties distribution for the primary and secondary streams along the ramjet duct. The distance x has been normalized by the ramjet duct length, thus $x = 0$ corresponds to station 3, and $x = 1$ corresponds to station 6. This figure shows that the primary and secondary pressures are matched within a couple of grid-points. At the Mach-1 condition, the rocket flow is underexpanded and therefore must expand rapidly to match the secondary stream pressure. As a result, the primary Mach number increases and the static temperature decreases. Further downstream, the primary Mach number continues to increase gradually through the expanding ramjet duct at the same time that the temperature decreases. At the Mach-2 condition, the rocket is overexpanded and its pressure must be brought up to that of the secondary stream. The rapid rise in primary pressure and temperature (and a decrease in Mach number) is the one dimensional approximation of an oblique shock. The pressure in the ramjet duct remains high until the heat release causes the pressure to fall. For both of these cases, the secondary stream thermally chokes at a location corresponding approximately to the end of the heat release (maximum secondary flow temperature).

Figure 8 shows a typical convergence history for the primary and secondary flows. For all cases presented, the calculations were stopped when both norms were smaller than 10^{-6} . Experience showed that continuing the computations far beyond this convergence level resulted in only negligible changes in the performance parameters (less than half a percent).

Figure 9 shows the net specific impulse variation with free-stream Mach number for various rocket chamber pressure ratios. The effect of ramjet cycle efficiency is evident above Mach 1.5. Also apparent is the trend toward higher specific impulse as the rocket chamber pressure is reduced. The dip in specific impulse at Mach 1 is due to inlet drag.

Figure 10 shows the variation of net thrust coefficient, defined as $C_t = F_{net}/(p_0 A_c)$, with Mach number. Above Mach 1.5, the percentage of thrust produced by the ramjet increases rapidly. Therefore, as the vehicle accelerates, the rocket can be throttled down to increase the efficiency. When the ramjet thrust alone is sufficient for adequate acceleration, the rocket can be completely shut off. Therefore, a smooth transition from rocket propulsion at lift-off to ramjet propulsion at some design supersonic Mach number can be accomplished.

Figure 11 shows the ratio of the secondary to primary flow, β , defined as

$$\beta = \frac{(\dot{m}_{air} + \dot{m}_{fuel})_s}{\dot{m}_p} \quad (25)$$

For clarity, the plot is presented only for the highest and lowest chamber pressures considered in the study. The results indicate that at high supersonic speeds, and low rocket chamber pressure, the secondary flow can be up to 25 times larger than the rocket flow.

At each Mach number between Mach 1 and Mach 2.5, a different fuel-air ratio was needed for each value of the rocket chamber pressure in order to keep the airflow fixed at the inlet critical value. More fuel is required at the lower chamber pressures. Figure 12 shows the required equivalence ratio as a function of Mach number for the various chamber pressures. Below a Mach number of 1.0, the air-stream is not fueled since there is not enough ram pressure for efficient ramjet operation. At Mach 2.5 and above, the fuel-air ratio reaches stoichiometric proportions for all chamber pressures. From Mach 1 to Mach 2, the same heat distribution given in Eq. 19 was used with $x_q^{st} = 0.2$, and $x_q^{en} = 0.95$. The thermal throat for all these cases was established just ahead of x_q^{en} , going from $x^* = 0.94$ at Mach-1 to $x^* = 0.90$ at Mach-2. For Mach numbers above 2.5, where the secondary stream was already at stoichiometric proportions, it was necessary to move the thermal throat upstream in order to match the prescribed airflow. This was accomplished by moving the ignition point upstream and shortening the heat release zone. The thermal throat location was approximately $x^* = 0.77$ for Mach 2.5, and $x^* = 0.45$ for Mach 3.

Figures 13 and 14 show the variation of specific impulse and net thrust coefficient with equivalence ratio at various Mach numbers, and for a rocket chamber pressure of $p_c/p_0 = 200$. The inlet drag was assumed to be constant at each Mach number. The figures show that adding fuel at a Mach number of 0.5 does not generate any significant additional thrust. The benefits of adding fuel to the secondary stream begin to become evident at Mach 1. At higher Mach numbers, the specific impulse variation with equivalence ratio shows a rapid initial increase followed by a more gradual increase at higher values of the equivalence ratio. From an overall vehicle performance point of view this suggests that the optimum equivalence ratio should be near the "knee" of the curve ($\phi \approx 0.6$) since adding additional fuel results in only small increases in performance at the cost of larger, and heavier fuel tanks.

Figure 15 compares the specific impulse for the IRS and SMC cycles from lift-off to Mach 3, along a typical Trailblazer flight trajectory. The SMC calculations were carried out using RAMSCRAM¹¹, a control-volume type cycle anal-

ysis code for ramjet and scramjet engines, including ejector modeling. The SMC calculations were carried out using the same rocket chamber pressures (listed in Fig. 16), and the same values for the various efficiency parameters (i.e., inlet recovery, combustion efficiency, nozzle gross thrust coefficient, etc.). In addition, the SMC calculations assumed complete mixing and chemical equilibrium at the thermal throat, and assumed no inlet losses at sea level static conditions. Similar to the calculations for the IRS cycle, the SMC analysis assumed flow expansion to atmospheric pressure at station 9 (see Fig. 2b).

The IRS cycle is slightly less efficient than its counterpart SMC cycle up to around Mach 3, where the two curves cross over. The differences in net specific impulse are in general less than 10%, with a maximum of 17% occurring at Mach 1. This difference in low speed performance would result in a 2-3% change in the launch vehicle final mass. Advantages in weight and simplicity of the IRS cycle may more than compensate for the lower cycle efficiency.

Conclusions

The numerical model developed in this study is an efficient approach for analyzing the performance of the IRS cycle. Computations of benchmark test cases for reacting and nonreacting flows, carried out with the present numerical method, were in excellent agreement with exact analytical results. Shock waves were sharply captured over two grid points.

The results obtained for the IRS cycle show that at subsonic speeds, there is no benefit in adding fuel to the airstream. The airflow, however, prevents the rocket plume from over-expanding. Above Mach 1, the airflow can be fueled and burned to generate ramjet thrust. The fraction of the thrust generated by the ramjet part of the combined cycle increases rapidly with Mach number, and the rocket can be progressively throttled down to obtain a higher specific impulse. When the ramjet thrust alone is sufficient, the rocket can be completely shut off. Therefore, a smooth transition from all-rocket at lift-off to pure ramjet at some design supersonic Mach number is naturally attained.

An optimum value of the equivalence ratio can be defined at each Mach number, above which only small increases in thrust and specific impulse occur. Operating above the optimum equivalence ratio may not be justified due to hydrogen tank size considerations.

Low speed operation of an RBCC engine requires the ability to control the inlet diffuser exit pressure in order to keep the inlet operating at optimum conditions through the

entire Mach number range. The IRS cycle can achieve this by adjusting the amount and radial distribution of fuel injected into the secondary stream, thereby controlling the location of the thermal throat.

Comparisons between the unmixed IRS cycle and the fully mixed SMC cycle showed that the IRS cycle performance was slightly lower than that of the SMC cycle. However, when other advantages of the IRS cycle, such as high structural efficiency, minimum system complexity and constant rocket O/F ratio are considered, the IRS cycle may be the best choice for an RBCC single-stage-to-orbit vehicle.

References

1. Trefny, C.J., "An Air-Breathing Launch Vehicle Concept for Single-Stage-to-Orbit," AIAA Paper 99-2730, 1999.
2. Escher, J.D., "A User's Primer for Comparative Assessments of All-Rocket and Rocket-Based Combined-Cycle Propulsion Systems for Advanced Earth-to-Orbit Space Transport Applications," AIAA Paper 95-2474, 1995.
3. Dimotakis, P.E., "Turbulent Free Shear Layer Mixing and Combustion," High-Speed Flight Propulsion Systems, S.N.B. Murthy and E.T. Curran editors, AIAA Progress in Astronautics and Aeronautics Series, Vol. 137, Washington, DC, 1991.
4. Yee, H.C., "Upwind and Symmetric Shock-Capturing Schemes," NASA TM-89464, 1987.
5. Radhakrishnan, K., "LSENS-A General Chemical Kinetics and Sensitivity Analysis Code for Homogeneous Gas-Phase Reactions," NASA RP 1328, January 1994.
6. Gordon, S. and McBride, B.J., "Computer Program for Calculation of Complex Chemical Equilibrium Compositions, Rocket Performance, Incident and Reflected Shocks, and Chapman-Jouguet Detonations," NASA SP-273, 1971.
7. Yee, H.C., "Construction of Explicit and Implicit Symmetric TVD Schemes and Their Applications," *Journal of Computational Physics*, Vol. 68, 1987, pp. 151-179
8. Debonis, J.R., Trefny, C.J. and Steffen, C.J., "Inlet Development for a Rocket-Based Combined-Cycle, Single Stage to Orbit Vehicle Using Computational Fluid Dynamics," AIAA Paper 99-2239, 1999.
9. Hill, P.G. and Peterson, C.R., *Mechanics and Thermodynamics of Propulsion*, Addison-Wesley, Reading, 1965.

10. Yungster, S., Eberhardt, S. and Bruckner, A.P., "Numerical Simulation of Hypervelocity Projectiles in Detonable Gases," *AIAA Journal*, Vol. 29, No. 2, Feb. 1991, pp. 187-199.

11. Burkardt, L.A. and Franciscus, L.C., "RAMSCRAM - A Flexible Ramjet/Scramjet Engine Simulation Program," NASA TM 102451, June 1990.

Appendix

For the quasi-one dimensional Euler equations, the flux Jacobian matrix A is given by

$$A = \begin{bmatrix} 0 & 1 & 0 \\ p_\rho - u^2 & u(2 - p_e) & p_e \\ u(p_\rho - H) & H - u^2 p_e & u(1 + p_e) \end{bmatrix} \quad (26)$$

Here H is the total enthalpy per unit mass

$$H = (e + p)/\rho \quad (27)$$

Note that the relation between pressure and the flow variables involves β which itself is a function of density and energy, and therefore complicates the computation of the partial derivatives in the Jacobian matrix. In the present work we utilize expressions for these partial derivatives obtained for the more general case of finite rate chemistry. The resulting expressions are (see Ref. 10):

$$p_e = \frac{R}{c_v} \quad (28)$$

$$p_\rho = RT(1 + p_e) + p_e(u^2 - H) \quad (29)$$

Here R and c_v denote the specific gas constant, and specific heat at constant volume for the mixture at the equilibrium conditions. The eigenvalues and eigenvectors of the Jacobian matrix are:

$$\Lambda = \text{Diag}[u - a, u, u + a] \quad (30)$$

where a is the frozen speed of sound defined by

$$a^2 = p_\rho + p_e(H - u^2) \quad (31)$$

$$X = \begin{bmatrix} 1 & 1 & 1 \\ u - a & u & u + a \\ (H - ua) & (u^2 - p_\rho/p_e) & (H + uc) \end{bmatrix} \quad (32)$$

$$X^{-1} = \begin{bmatrix} \frac{1}{2}(b_1 + u/a) & -\frac{1}{2}(ub_2 + 1/a) & \frac{1}{2}b_2 \\ 1 - b_1 & b_2u & -b_2 \\ \frac{1}{2}(b_1 - u/a) & -\frac{1}{2}(ub_2 - 1/a) & \frac{1}{2}b_2 \end{bmatrix} \quad (33)$$

where $b_1 = p_\rho/a^2$, and $b_2 = p_e/a^2$

Table 1: Nozzle gross thrust coefficient.

M_0	C_{fg}
0.0	0.95
0.5	0.925
1.0	0.90
1.5	0.925
2.0	0.95
2.5	0.95
3.0	0.95

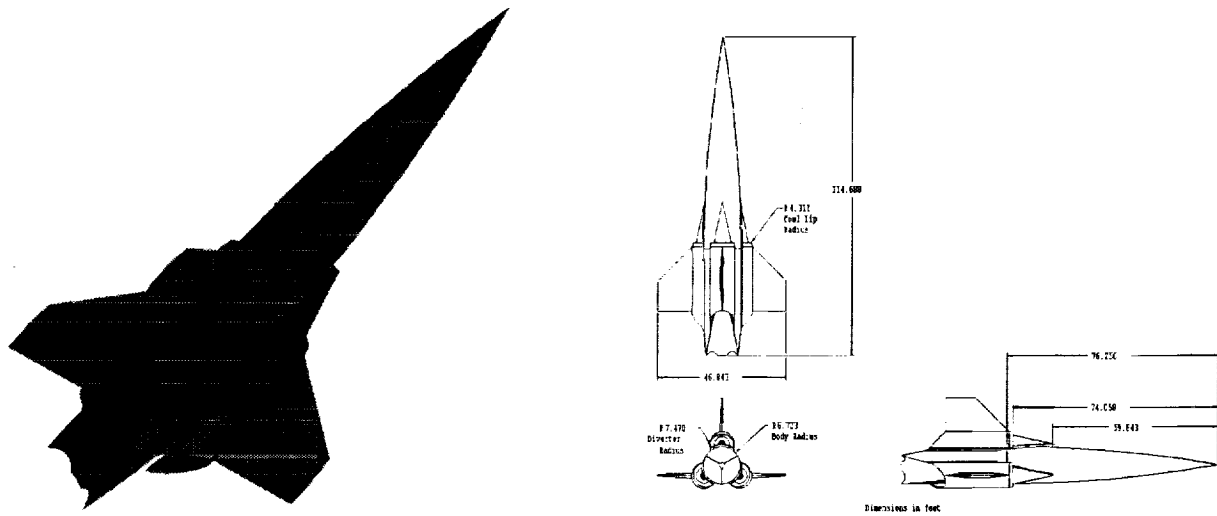
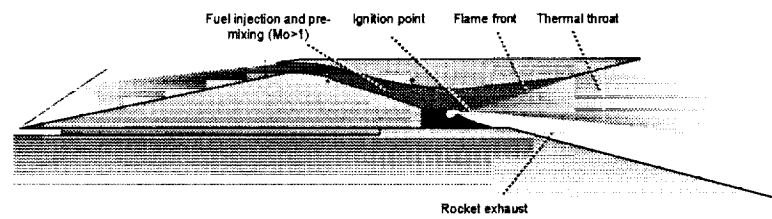
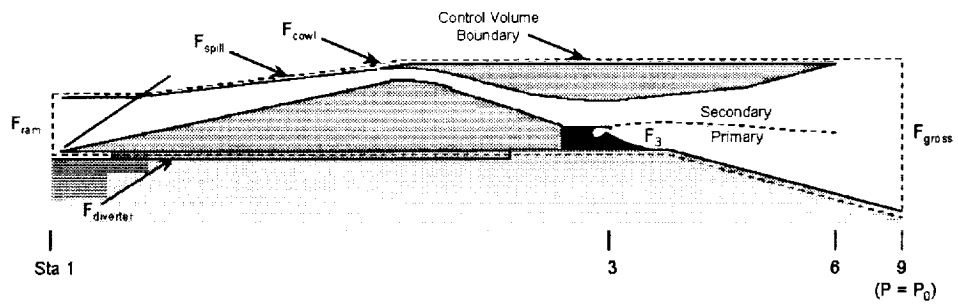


Figure 1. Trailblazer SSTO Vehicle.



(a)



(b)

Figure 2. Cross-sectional view of the Trailblazer engine.; (a) schematic of the Independent Ramjet Stream (IRS) propulsion mode, (b) Control Volume around the RBCC engine.

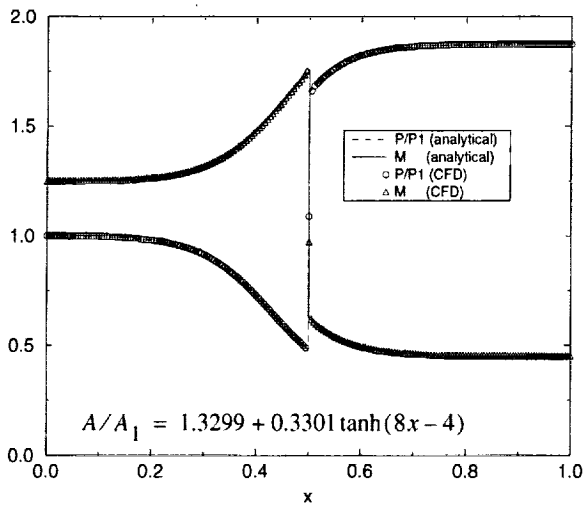


Figure 3. Numerical and exact solutions of ideal gas flow in a divergent nozzle.

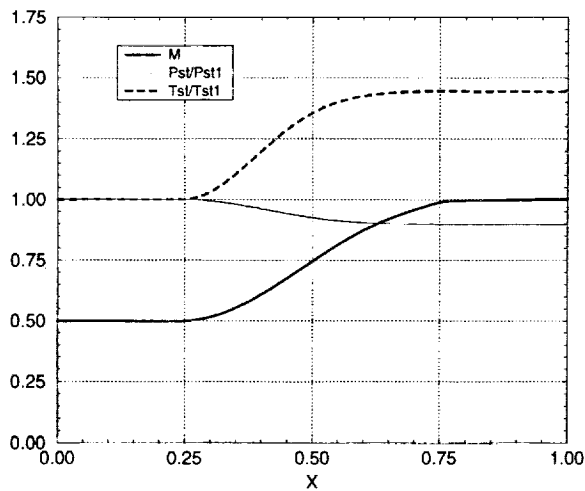


Figure 4. Variation of Mach number, total pressure and total temperature in Rayleigh Flow (ideal gas).

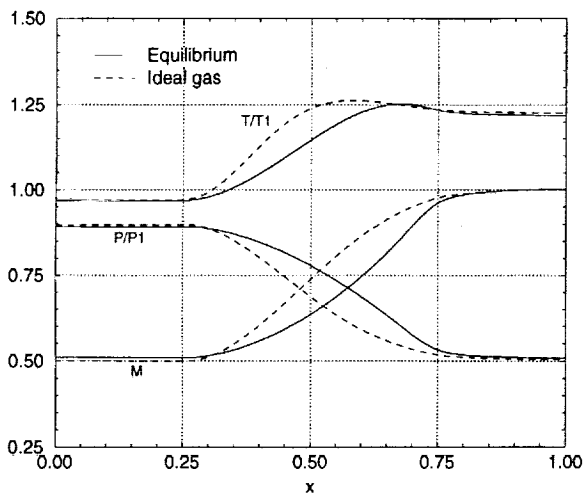


Figure 5. Comparison between equilibrium and ideal gas calculations for Rayleigh Flow. ($P_1=1.0$ atm., $T_1=404.7$ K are reference values.)

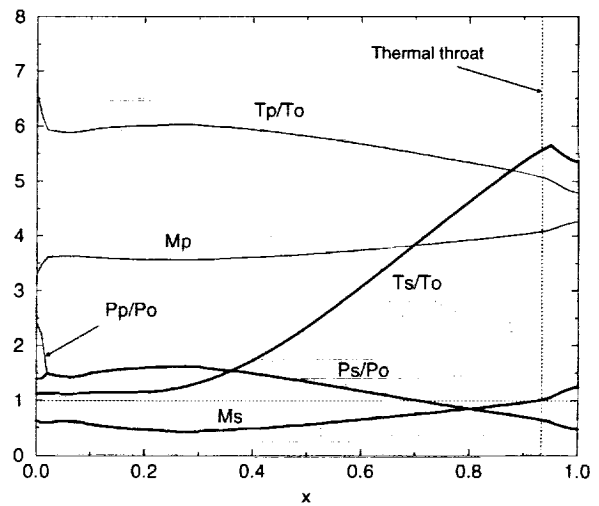


Figure 6. Pressure, temperature and Mach number distribution for $M_0 = 1$, $p_c/p_0 = 200$. Subscripts are: p- primary, s- secondary, 0- free-stream.

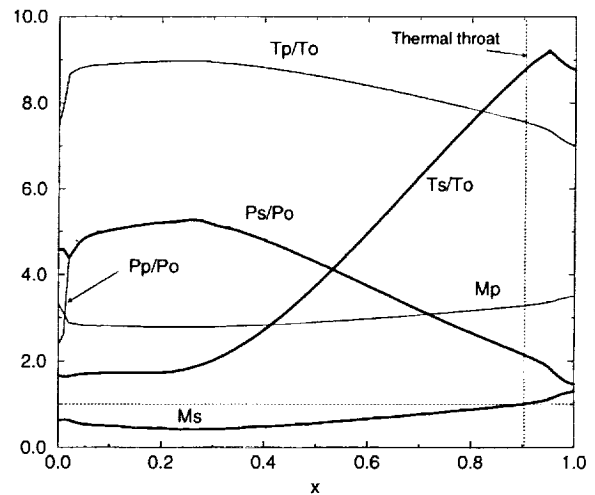


Figure 7. Pressure, temperature and Mach number distribution for $M_0 = 2$, $p_c/p_0 = 200$.

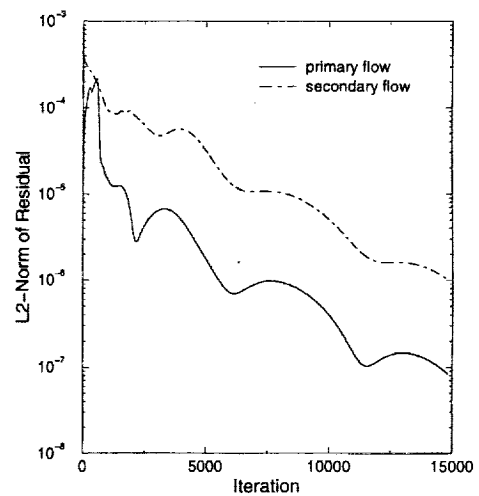


Figure 8. Convergence history for primary and secondary flows.

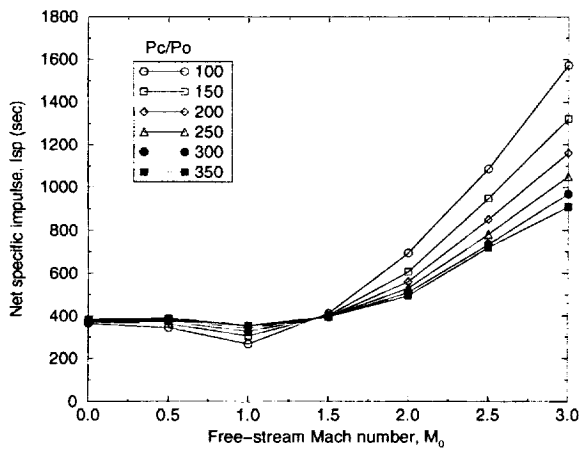


Figure 9. Net specific impulse as a function of free stream Mach number for various rocket chamber pressure ratios.

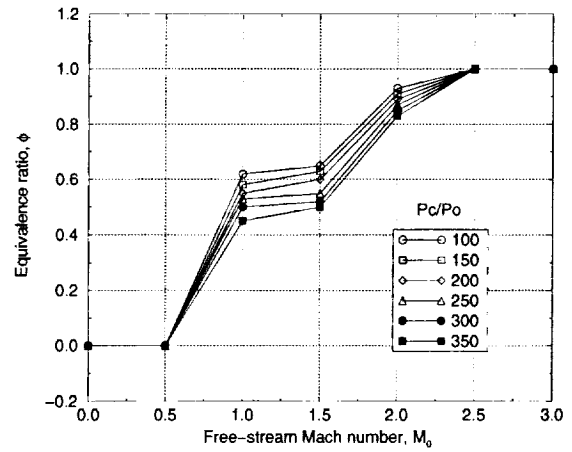


Figure 12. Equivalence ratio as a function of free stream Mach number for various rocket chamber pressure ratios.

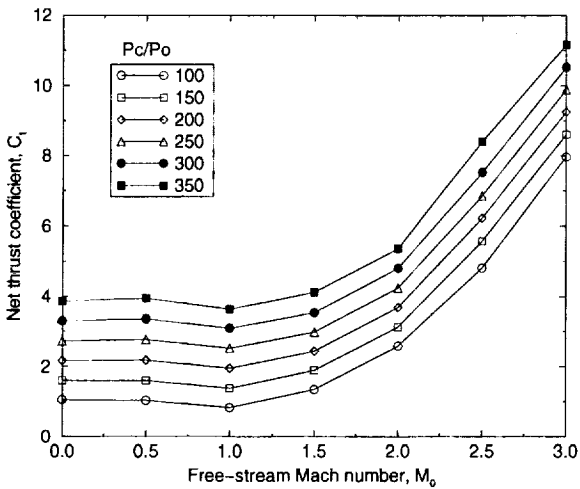


Figure 10. Net thrust coefficient as a function of free stream Mach number for various rocket chamber pressure ratios.

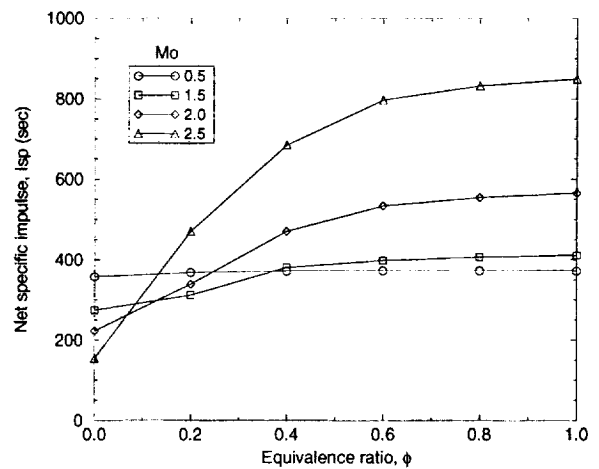


Figure 13. Net specific impulse as a function of equivalence ratio for various free-stream Mach numbers $p_c/p_0 = 200$.

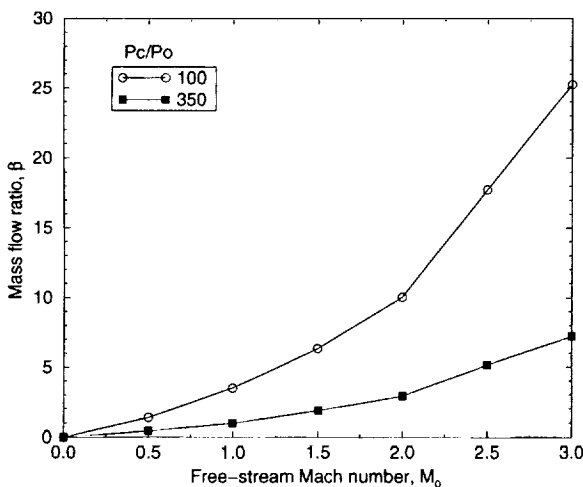


Figure 11. Ratio of secondary to primary flow as a function of free stream Mach number for two rocket chamber pressure ratios.

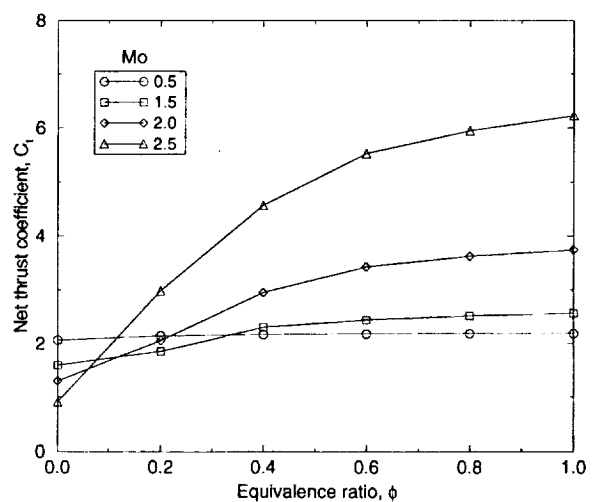


Figure 14. Net thrust coefficient as a function of equivalence ratio for various free-stream Mach numbers, $p_c/p_0 = 200$.

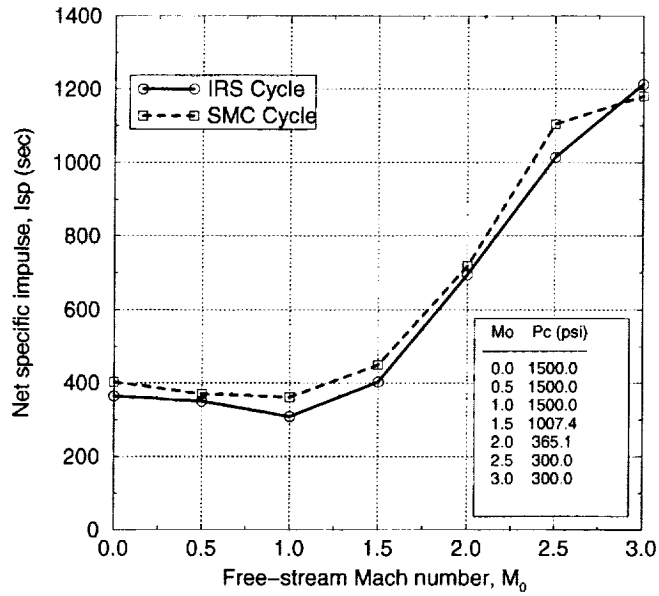


Figure 15. Net specific Impulse comparison for IRS and SMC cycles along a typical Trailblazer trajectory from lift-off to Mach 3.



REPORT DOCUMENTATION PAGE

Form Approved
OMB No. 0704-0188

Public reporting burden for this collection of information is estimated to average 1 hour per response, including the time for reviewing instructions, searching existing data sources, gathering and maintaining the data needed, and completing and reviewing the collection of information. Send comments regarding this burden estimate or any other aspect of this collection of information, including suggestions for reducing this burden, to Washington Headquarters Services, Directorate for Information Operations and Reports, 1215 Jefferson Davis Highway, Suite 1204, Arlington, VA 22202-4302, and to the Office of Management and Budget, Paperwork Reduction Project (0704-0188), Washington, DC 20503.

1. AGENCY USE ONLY (Leave blank)		2. REPORT DATE September 1999	3. REPORT TYPE AND DATES COVERED Contractor Report	
4. TITLE AND SUBTITLE Analysis of a New Rocket-Based Combined-Cycle Engine Concept at Low Speed			5. FUNDING NUMBERS WU-505-90-5K-00 NCC3-542	
6. AUTHOR(S) S. Yungster and C.J. Trefny				
7. PERFORMING ORGANIZATION NAME(S) AND ADDRESS(ES) Institute for Computational Mechanics in Propulsion 22800 Cedar Point Road Cleveland, Ohio 44142			8. PERFORMING ORGANIZATION REPORT NUMBER E-11824	
9. SPONSORING/MONITORING AGENCY NAME(S) AND ADDRESS(ES) National Aeronautics and Space Administration John H. Glenn Research Center at Lewis Field Cleveland, Ohio 44135-3191			10. SPONSORING/MONITORING AGENCY REPORT NUMBER NASA TM-1999-209393 AIAA 99-2393 ICOMP-99-05	
11. SUPPLEMENTARY NOTES Prepared for the 35th Joint Propulsion Conference and Exhibit cosponsored by AIAA, ASME, SAE, and ASEE, Los Angeles, California, June 20-24, 1999. S. Yungster, Institute for Computational Mechanics in Propulsion, NASA Glenn Research Center, Cleveland, Ohio 44135; C.J. Trefny, NASA Glenn Research Center. ICOMP Program Director, Lou Povinelli, organization code 5880, (216) 433-5818.				
12a. DISTRIBUTION/AVAILABILITY STATEMENT Unclassified - Unlimited Subject Category: 20 This publication is available from the NASA Center for AeroSpace Information, (301) 621-0390.			12b. DISTRIBUTION CODE Distribution: Nonstandard	
13. ABSTRACT (Maximum 200 words) An analysis of the Independent Ramjet Stream (IRS) cycle is presented. The IRS cycle is a variation of the conventional ejector-ramjet, and is used at low speed in a rocket-based combined-cycle (RBCC) propulsion system. In this new cycle, complete mixing between the rocket and ramjet streams is not required, and a single rocket chamber can be used without a long mixing duct. Furthermore, this concept allows flexibility in controlling the thermal choke process. The resulting propulsion system is intended to be simpler, more robust, and lighter than an ejector-ramjet. The performance characteristics of the IRS cycle are analyzed for a new single-stage-to-orbit (SSTO) launch vehicle concept, known as "Trailblazer." The study is based on a quasi-one-dimensional model of the rocket and air streams at speeds ranging from lift-off to Mach 3. The numerical formulation is described in detail. A performance comparison between the IRS and ejector-ramjet cycles is also presented.				
14. SUBJECT TERMS Single stage to orbit vehicles; Chemical equilibrium flows; Computational fluid dynamics			15. NUMBER OF PAGES 18	
			16. PRICE CODE A03	
17. SECURITY CLASSIFICATION OF REPORT Unclassified	18. SECURITY CLASSIFICATION OF THIS PAGE Unclassified	19. SECURITY CLASSIFICATION OF ABSTRACT Unclassified	20. LIMITATION OF ABSTRACT	